ARTICLE

Highly Sensitive and Wearable In$_2$O$_3$ Nanoribbon Transistor Biosensors with Integrated On-Chip Gate for Glucose Monitoring in Body Fluids

Qingzhou Liu,[†] Yihang Liu,[‡] Fanqi Wu,[†] Xuan Cao,[†] Zhen Li,[‡] Mervat Alharbi,[§] Ahmad N. Abbas,[∥,⊥] Moh R. Amer,*[§,#] and Chongwu Zhou*[†,‡]

[†]Mork Family Department of Chemical Engineering and Materials Science and [‡]Ming Hsieh Department of Electrical Engineering, University of Southern California, Los Angeles, California 90089, United States

[§]Center of Excellence for Green Nanotechnologies, Joint Centers of Excellence Program, King Abdulaziz City for Science and Technology, P.O Box 6086, Riyadh 11442, Saudi Arabia

[∥]Department of Electrical and Computer Engineering, University of Jeddah, 285 Dhahban 23881, Saudi Arabia

[⊥]Department of Electrical and Computer Engineering, King Abdulaziz University, Abdullah Sulayman Street, Jeddah 22254, Saudi Arabia

[#]Department of Electrical Engineering, University of California, Los Angeles, 420 Westwood Plaza, 5412 Boelter Hall, Los Angeles, California 90095, United States

S Supporting Information

ABSTRACT: Nanoribbon- and nanowire-based field-effect transistor (FET) biosensors have stimulated a lot of interest. However, most FET biosensors were achieved by using bulky Ag/AgCl electrodes or metal wire gates, which have prevented the biosensors from becoming truly wearable. Here, we demonstrate highly sensitive and conformal In$_2$O$_3$ nanoribbon FET biosensors with a fully integrated on-chip gold side gate, which have been laminated onto various surfaces, such as artificial arms and watches, and have enabled glucose detection in various body fluids, such as

sweat and saliva. The shadow-mask-fabricated devices show good electrical performance with gate voltage applied using a gold side gate electrode and through an aqueous electrolyte. The resulting transistors show mobilities of ~22 cm^2 V^{-1} s^{-1} in 0.1× phosphate-buffered saline, a high on−off ratio (10^5), and good mechanical robustness. With the electrodes functionalized with glucose oxidase, chitosan, and single-walled carbon nanotubes, the glucose sensors show a very wide detection range spanning at least 5 orders of magnitude and a detection limit down to 10 nM. Therefore, our high-performance In$_2$O$_3$ nanoribbon sensing platform has great potential to work as indispensable components for wearable healthcare electronics.

KEYWORDS: wearable biosensor, gold side gate, glucose sensor, indium oxide semiconductor, field-effect transistor, shadow-mask fabrication
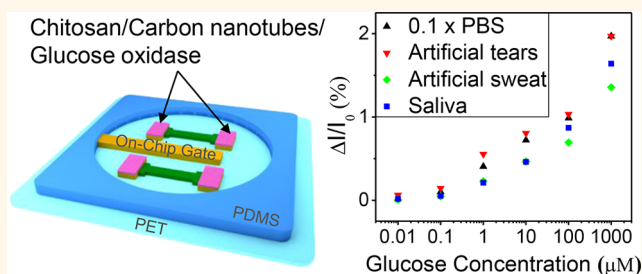
Wearable biosensors are smart electronic devices that can be worn on the body as implants or accessories. Recent advances in microelectronics, telecommunications, and sensor manufacturing have opened up possibilities for using wearable biosensors to continuously monitor an individual's body status without interrupting or limiting the user's motions.[1−8] However, while many commercially available wearable electronics can track users' physical activities, devices that can provide an insightful view of user's health status at the molecular level need more development. On the other hand,

although some commercial hand-held analyzers enable glucose or lactate detection, most of these devices rely on blood samples.[9] Neither finger-prick nor invasive sensors (such as a needle embedded under the skin) are desired for wearable biomedical applications. Continuous analyte monitoring, a key advantage offered by wearable biosensors, has great potential in
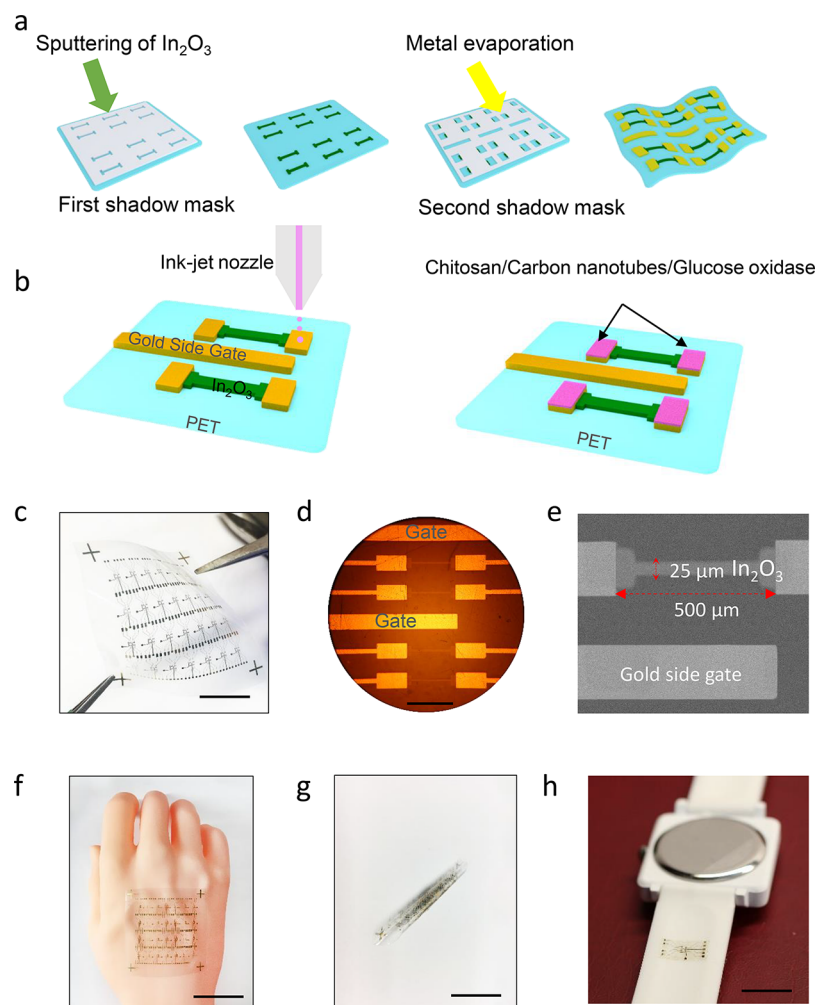
A

Figure 1. (a) Schematic diagrams showing the fabrication procedure of In_2O_3 FETs on a PET substrate using two-step shadow masks. (b) Schematic diagrams of functionalization on the surface of the electrodes using inkjet printing. (c) Photograph of as-fabricated In_2O_3 FETs. Scale bar is 1 cm. (d) Optical image showing a group of In_2O_3 biosensors with two gold side gate electrodes. Scale bar is 500 μm. (e) SEM image of an In_2O_3 nanoribbon devices (L = 500 μm, W = 25 μm) and a gold side gate electrode (W = 150 μm). (f) Photograph of In_2O_3 FET foil laminated on an artificial human hand. Scale bar is 3 cm. (g) In_2O_3 biosensor foil in a rolled-up state. Scale bar is 3 cm. (h) Photograph of an In_2O_3 FET chip attached onto the back casing of a watch. Scale bar is 1 cm.

many cases. For example, optimum diabetes management needs regular glucose monitoring, and a trend of glucose level is more meaningful than an accurate data point.[10] Besides glucose monitoring, real-time detection of some pathogens in body fluids can warn of the possible onset of certain diseases.[11]

Although blood is by far the most understood sample for diagnosis, other biological fluids such as sweat, tears, and saliva also contain tremendous biochemical analytes that can provide valuable information and are more readily accessible compared to blood.[10,12] Recent studies suggest a diagnosis system based on the glucose concentration in body fluids to estimate blood glucose levels.[13−15] However, many challenges still exist for the accurate glucose sensing in body fluids.[16,17] For example, the glucose levels in body fluids are much lower than that in blood.[18] The sensing results can be affected by ambient temperature changes, mechanical deformation caused by body motion, and the sample collection procedure.

Among various types of sensors (*e.g.*, optical, piezoelectric, and electrochemical sensors), electrochemical sensors are the most promising candidate for wearable technology owing to their high performance, portability, simplicity, and low

cost.[19−24] Considering the demands of wearable biosensors, the selection of the sensing platform is critical to high sensitivity and reproducibility, real-time detection, and simple integration with wearable environments (*e.g.*, human skin, tooth, and eye).[11,25] Nanobiosensors based on indium oxide (In_2O_3) field-effect transistors (FETs) are well suited for wearable biosensor applications because of the quick response time for real-time and continuous monitoring, large detectable concentration range, high sensitivity, high uniformity for reliable sensing, and the capability to integrate with other microfluidic and electronic functional groups.[26−30] Furthermore, the exposed semiconductor channel regions can be modified with various functional groups or receptors easily and thus make the In_2O_3 nanobiosensors suitable for multiplexed sensing.

The current FET-based biosensor platform is usually composed of individual sensors with an external Ag/AgCl solution gate electrode to set the operational point of the sensors to the optimal detection mode. In order to build a wearable biosensor platform, a stand-alone sensor array is desired. The Ag/AgCl electrode is commonly used as the

reference electrode in the electrochemical measurements and biosensing applications because it can provide stable potential and can read signals precisely. However, the integration of the Ag/AgCl electrode into a biosensor chip remains challenging. For FET-based biosensors, the gate electrode only needs to supply stable gate bias to the devices, which can be achieved by an on-chip metal side electrode. The source–drain electrodes and the on-chip gate electrodes can be incorporated into the straightforward two-step shadow-mask fabrication process so that no additional fabrication steps are required. The integration of In_2O_3 glucose sensors with wearable electronics can generate high impact for diabetes monitoring, since diabetes is one of the most prevalent and pressing diseases in the world. Moreover, the development of wearable sensors for *in situ*, real-time, and low-cost detection of biologically and medically important targets will generate broad impact in many applications involving electronic skin,[31] thermal regulation,[32] chemical sensing,[33] and the detection of pathogens in body fluids.[11]

Here, we demonstrate highly sensitive and conformal In_2O_3 nanoribbon FET biosensors with a fully integrated on-chip gold side gate, which have been laminated onto various surfaces, such as artificial arms and watches, and have enabled glucose detection in various body fluids, such as sweat and saliva. The devices are fabricated through two shadow masks. First, a shadow mask is used to define the sputter-coating of In_2O_3 nanoribbons, and the second shadow mask is used for metal deposition of the source, drain, and side gate. The source and drain electrodes are modified with the enzyme glucose oxidase (GOx), biocompatible polymer chitosan, and single-walled carbon nanotubes (SWCNTs) using inkjet printing. The gold side gated In_2O_3 FETs show good electrical performance on highly flexible substrates. The optimized glucose sensors show a very wide detection range spanning at least 5 orders of magnitude and detection limits down to 10 nM. The noninvasive glucose detections in human body fluids, such as tears and sweat, and the sensing on artificial skin and eye replicas are demonstrated. Therefore, this type of device is a highly sensitive platform for not only glucose detections but also many other types of sensing applications.

RESULTS AND DISCUSSION

The In_2O_3 nanoribbon devices were fabricated following our previous reported shadow-mask fabrication technique;[26] however, this time we have added side gate patterns to the source/drain shadow mask and have used a 5 μm ultraflexible PET substrate. Figure 1a illustrates the scheme for fabricating flexible In_2O_3 macroelectronics on PET substrates. First, a PET substrate was attached to the first shadow mask using antistatic tape. Then we used radio frequency (RF) sputtering to deposit 16 nm thick In_2O_3 nanoribbons through the openings on the shadow mask. The second shadow mask was then laminated onto the PET substrate for the following metal deposition. After using a single mask to define the source, drain, and side gate electrodes, the as-made biosensor foil was peeled off from the shadow mask for further electrical characterization. While most previous glucose-sensing studies used electrochemical sensors with large working electrodes by functionalizing the electrodes with drop casting,[2,8] here, we have developed an inkjet printing technique to functionalize our FET In_2O_3 glucose biosensors, as shown in Figure 1b. Due to the small dimensions (~25 μm × 500 μm) of our nanoribbon biosensors, the traditional drop-cast deposition method causes the whole

active sensing area to be covered by the chitosan film. In order to keep the channel area exposed, we employed a SonoPlot printer with a 50 μm glass nozzle to print the chitosan ink only on the source and drain pads. The ink was made of chitosan, single-walled carbon nanotubes, and glucose oxidase, and the preparation of the ink is described in detail in the Experimental Methods section. Figure 1c shows a photograph of an as-fabricated In_2O_3 biosensor foil with a size of 5 cm × 5 cm. An optical image of a group of In_2O_3 biosensors and two gold side gate electrodes is shown in Figure 1d. Figure 1e shows a scanning electron microscope (SEM) image of the channel region and the gold side gate of a biosensor. To further characterize the In_2O_3 nanoribbons, we used atomic force microscopy (AFM) and X-ray diffraction (XRD) on samples deposited on a polyethylene terephthalate (PET) substrate (Figure S1). The AFM images show that the nanoribbons are solid and have clear edges. The height profile shows the thickness of In_2O_3 nanoribbons is ~20 nm. The XRD pattern shown presents only PET peaks, indicating the In_2O_3 is amorphous. Figure 1f shows the fabricated In_2O_3 nanoribbon FET foil was conformably laminated onto an artificial human hand, indicating the bendability and wearability of the In_2O_3 nanoribbon biosensors. Figure 1g exhibits the biosensor foil rolled up with a radius of curvature of ~1 mm. The flexible biosensor can be further attached onto the back casing of a watch (Figure 1h), showing the concept that such In_2O_3 transistor biosensors can be integrated with smart watches in the future. We believe that flexible, lab-on-a-chip, and conformal In_2O_3 nanoribbon electronics are highly advantageous for wearable biosensor applications.

In many previous studies, a Ag/AgCl electrode is commonly used as the reference electrode in electrochemical measurements and biosensing applications because it can provide stable potential and can also read voltage precisely. However, the integration of the Ag/AgCl electrode onto a biosensor chip increases the steps and difficulty of fabrication. Herein, we have replaced the Ag/AgCl external electrode with a gold side gate to supply gate bias to the devices. There are two gold side gate electrodes in a group of four In_2O_3 FET devices. The one in the middle will replace the Ag/AgCl external liquid gate to supply gate voltage, and the other one at the rear can be used to monitor changes in potential on the devices. We first compared the device performance with gate voltage applied by the external Ag/AgCl electrode and the on-chip gold side electrode. Here, all the measurements were done when the device active area was immersed into a microwell filled with 300 μL of electrolyte solution (0.1× phosphate buffered saline (PBS)). Figure 2a and b show family curves of drain current–gate voltage ($I_{DS}-V_{GS}$) and drain current–drain voltage ($I_{DS}-V_{DS}$) when the gate voltage was biased through a Ag/AgCl electrode. The schematic diagram of the measurement setup is shown in the inset of Figure 2a. The performance of the gold side gate controlled In_2O_3 FET is presented in Figure 2c ($I_{DS}-V_{GS}$) and d ($I_{DS}-V_{DS}$). The output and transfer curves of the FET devices demonstrate that the In_2O_3 nanoribbon devices can work properly under gate bias supplied by the gold side gate. The output characteristics of the FET devices demonstrated ohmic behavior with a good linear regime in the "on" state, and the drain current got saturated when the bias increased further. All the curves in Figure 2b and d passing through the origin point indicate the minimal contribution of the gate leakage current to the drain current. The field-effect mobility of the
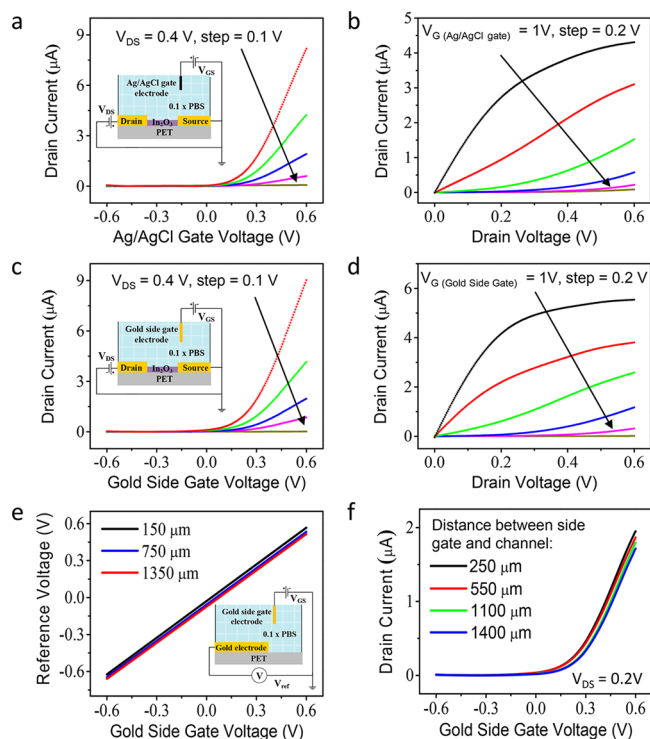
Figure 2. Electrical characterization of In$_2$O$_3$ nanoribbon biosensors using gold side gate electrodes. (a) Drain current *versus* Ag/AgCl gate voltage with drain voltage changing from 0.4 V to 0 V in steps of 0.1 V. Inset shows the schematic diagram of the measurement setup. (b) Family of I_{DS}−V_{DS} curves measured with a Ag/AgCl gate electrode. (c) Drain current *versus* gold side gate voltage with drain voltage varying from 0.4 to 0 V in steps of 0.1 V. (d) Family curves of I_{DS}−V_{DS} measured with gold side gate voltage varying from 1 V to 0 V in steps of 0.2 V. (e) Reference voltage measured with a gold electrode *versus* the gold side gate voltage. (f) Transfer characteristics of a representative FET with different gate-to-channel distances under V_{DS} = 0.2 V.

In$_2$O$_3$ FET is extracted to be 22.34 ± 1.44 cm^2 V^{-1} s^{-1} using the following equation:

$$g_m = \frac{dI_D}{dV_{GS}} = \frac{W}{L} C_{DL} \mu_{FE} V_D \tag{1}$$

where W is the channel width, L is the channel length, and C_{DL} is the electrical double layer capacitance per unit area in 0.1 M ionic strength aqueous solution reported previously (25.52 μF cm^{-2}).[34] The maximum transconductance of 5.69 μS was obtained at a drain voltage of 0.2 V and a gate voltage of 0.527 V (Figure S2 in the Supporting Information). To further confirm the gate control of the on-chip side gate electrode, we used one electrode as the gate bias supplier and another one as a reference electrode to monitor the actual change of potential on the devices, as the scheme shows in the inset of Figure 2e. In Figure 2e, we plotted the reference voltage (V_{REF}) against the gold side gate voltage (V_{GS}) with different distances between those two electrodes, 150, 750, and 1350 μm, respectively. It shows that V_{REF} is almost identical to V_{GS} regardless of the distance. We further plotted drain current *versus* gate bias applied through the gold side gate at different distances (Figure 2f), and the curves show negligible differences. A statistical study of key electrical properties for 50 In$_2$O$_3$ nanoribbon devices comparing the gate biased through the Ag/AgCl electrode and the gold side gate was conducted. Figure S3 in

the Supporting Information exhibits the device performance including mobility (μ), threshold voltage (V_{th}), on/off ratio, and on-state current, which are very similar to each other, which implies that the gold side gate and the Ag/AgCl gate can give an analogous gating effect. From all these figures of merit, we can conclude that the on-chip gate electrode has great control over the nanoribbon transistors in an aqueous environment.

In order to characterize the flexibility of the wearable In$_2$O$_3$ FETs, bending tests were carried out. As shown in Figure 3a,
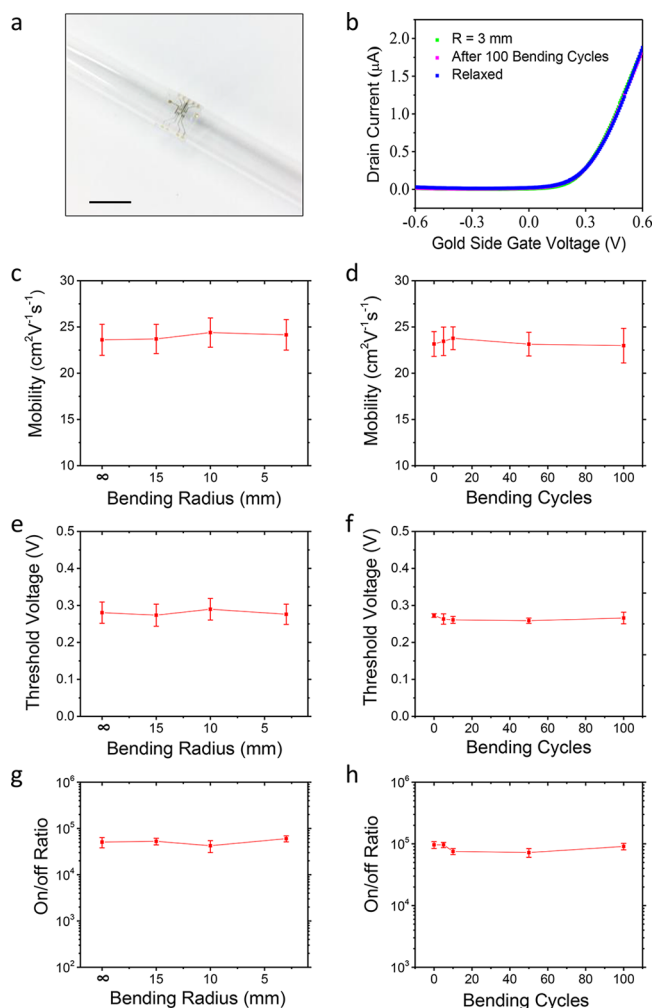

Figure 3. Flexibility of In$_2$O$_3$ FETs on a PET substrate. (a) Photograph of a biosensor foil wrapping around a glass cylinder. Scale bar is 5 mm. (b) Transfer characteristics of a representative In$_2$O$_3$ FET under a relaxed state, bent with a radius of ∼3 mm, and after bending 100 times. (c) Mobility, (e) threshold voltage, and (g) on−off ratio of In$_2$O$_3$ FETs bent with different radii. (d) Mobility, (f) threshold voltage, and (h) on−off ratio of In$_2$O$_3$ FETs bent with a radius of ∼3 mm after different bending cycles.

we tightly wrapped our fabricated In$_2$O$_3$ foil around a cylinder. The electrical performance of the devices under tensile strain was measured. Figure 3b compares the transfer characteristics of a representative In$_2$O$_3$ nanoribbon FET in three conditions: relaxed status, bent with a radius of curvature of ∼3 mm, and after 100 bending cycles. The devices exhibited n-type behavior in all three conditions without any perceptible change of its performance. In order to verify the reliability of our platform when deformed, the flexibility tests were performed on In$_2$O$_3$

FETs functionalized with a gel film containing chitosan, SWCNTs, and glucose oxidase. Figure 3c, e, and g plot the mobility, the on−off ratio, and the threshold voltage averaged over nine devices bent with a radius of curvature of infinity (relaxed) and 3, 10, and 15 mm, respectively. The typical transfer curves of the devices under different bending conditions are plotted in Figure S4 in the Supporting Information. When the foil was bent with a radius of curvature of ∼3 mm, a tensile strain of ∼0.25% (Supporting Information, S5), parallel to the drain-to-source current direction, was applied to the In_2O_3 FETs. We have further plotted out the mobility as a function of strain (Figure S5 in the Supporting Information). There was no significant change of the electrical performance of the In_2O_3 FETs when the devices were in different bending conditions, as the mobility only showed a small variation between 22.15 ± 1.68 and 22.70 ± 1.65 cm^2 V^{-1} s^{-1}, the threshold voltage only showed a variation between 0.273 ± 0.028 and 0.280 ± 0.027 V, and the logarithm on−off ratio showed a variation between 4.71 ± 0.13 and 4.84 ± 0.12. Figure 3d, f, and h plot the mobility, the threshold voltage, and the on−off ratio of the devices after 0 (before bending), 5, 10, 50, and 100 bending cycles, respectively, and the changes in device performance were negligible as well. The mobility varied in the range of 22.98 ± 1.34 to 23.78 ± 1.87 cm^2 V^{-1} s^{-1}, the threshold voltage varied between 0.273 ± 0.005 and 0.266 ± 0.016 V, and the logarithm on−off ratio varied between 4.98 ± 0.17 and 4.96 ± 0.14. On the basis of the test results, all the In_2O_3 nanoribbon FETs after bending tests still maintained excellent performance, confirming that our platform is reliable under mechanical deformation.

The ability to sense in a small amount of liquid is crucial to wearable sensors, because of the limited amount of body fluids at regular intervals. A polydimethylsiloxane (PDMS) stamp was adopted as a microwell to accumulate body fluids (Figure 4a). It can also serve as a passivation layer to ensure reliable sensing without disturbance introduced by electrical contact of the metal lines with the body and body fluids. A mixture of curing agent and PDMS at a ratio of 1:10 was first spin-coated onto a silicon wafer before thermally curing at 80 °C for 1 h. After punching a hole with a diameter of 3 mm, the PDMS stamp was laminated onto the biosensor substrate by van der Waals force. To guarantee the biosensor can work properly in a limited amount of liquid, we filled the PDMS microwell with 10 μL of solution and performed electrical measurements using a gold side gate electrode. Figure 4b and c show the transfer curves and output curves of the In_2O_3 FETs measured with a gold side gate in the electrolyte of ∼10 μL of 0.1× PBS. The electrical performance measured in a small amount of liquid is comparable to the results shown in Figure 2c and d (measured in 300 μL of 0.1× PBS). It illustrates that our biosensing platform can efficiently work in the liquid with an amount as small as 10 μL, which is a 30-fold decrease from what we previously reported.[26]

To further confirm the sensing ability of our biosensor platform, we conducted pH-sensing experiments to test the ionic sensitivity of the biosensor chip in responses to commercial pH solutions. Figure 4d shows the comparison of the pH sensing responses ($\Delta I/I_0$) with gate bias supplied using either a gold side electrode or a Ag/AgCl electrode. The responses are plotted as black up-triangles and red down-triangles for devices gated with a Ag/AgCl external liquid electrode and a gold side electrode, respectively. The baseline current I_0 was obtained when using 0.1× PBS (pH = 7.4) to
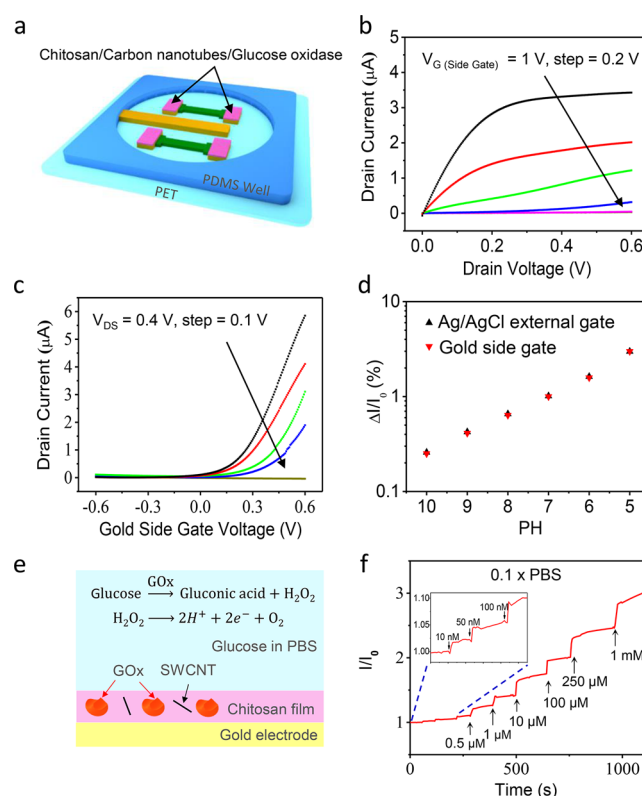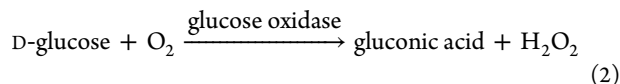

Figure 4. PH sensing and glucose sensing. (a) Schematic diagram showing a PDMS microwell attached to the PET substrate with In_2O_3 FETs. (b) Family curves of $I_{DS}-V_{DS}$ measured with the channel area submerged in the PDMS well. (c) Family curves of $I_{DS}-V_{GS}$ measured with the channel area submerged in the PDMS well. (d) PH sensing when the gate bias was applied with a Ag/AgCl electrode or a gold side gate electrode. (e) Schematic diagram showing the working principle of a glucose sensor. (f) Glucose sensing results in 0.1× PBS with a gold side gate.

stabilize the device, and then the PBS was sequentially changed to commercial pH buffer solutions ranging from pH 10 to pH 5. The devices showed an increase in conduction when the pH value of the solution decreased, because hydroxyl groups on the nanoribbon surface were protonated due to more H$^+$ ions in the solution, resulting in a positive gating effect on the channel area of the n-type In_2O_3 nanoribbon transistor. As observed, the sensing results from two different gate electrodes are almost identical to each other. They both are exponentially dependent on pH changes, and the drain current increased ∼2.4 times when the pH value increased by 1. The representative real-time sensing results are shown in Figure S6 in the Supporting Information.

After ensuring that our devices has good electrical performance and ionic sensitivity with the gold side gate, the In_2O_3 nanoribbon biosensors were used to detect D-glucose. Figure 4e shows a schematic diagram depicting the working principle of the glucose determination using In_2O_3 nanoribbon biosensors. The surfaces of the source and drain electrodes were functionalized with chitosan/carbon nanotubes/glucose oxidase using inkjet printing (see Experimental Methods for details). Chitosan is chosen to work as the immobilization layer since it is a biocompatible polymeric matrix with good film-forming ability and high water permeability.[24] Carbon nanotubes have been reported as efficient routes for increasing the sensitivity for many types of sensors, owing to their good electrocatalytic

property and capacity for biomolecule immobilization.[24,35,36] After being immobilized by the chitosan film and carbon nanotubes, the glucose oxidase enzymes accept electrons when they interact with glucose in the solution and thereafter transfer electrons to molecular oxygen, consequently producing hydrogen peroxide (H_2O_2). The enzymatically produced H_2O_2 will be oxidized under a bias voltage. The reactions are as follows:

$$D\text{-glucose} + O_2 \xrightarrow{\text{glucose oxidase}} \text{gluconic acid} + H_2O_2 \tag{2}$$

$$H_2O_2 \rightarrow O_2 + 2H^+ + 2e^- \tag{3}$$

The generation of H^+ depends on the concentration of glucose. Decreasing of the pH leads to protonation of the OH groups on the In_2O_3 surface and results in changes in the local FET electric field, ultimately causing changes in the conductance and current. Figure 4f shows the continuous monitoring of the sensing signal in responses to different glucose concentrations. The channel current increases with the additions of glucose and shows the detection limit of about 10 nM (~2.2% of the baseline current). Our glucose sensor can detect glucose in the concentration range between 10 nM and 1 mM, covering typical glucose concentrations in human body fluids. These glucose concentrations correspond to typical sweat glucose concentrations of both diabetes patients and healthy people.[10] The detection limit we obtained here is much lower than a typical electrochemical amperometric glucose sensor.[2,8] We also performed control experiments on sensors without glucose oxidase, and as observed, those sensors did not respond to glucose (Figure S7 in the Supporting Information).

Wearable In_2O_3 nanoribbon glucose sensors are further used for human body fluid analysis. The glucose concentration is much lower in tears, sweat, and saliva than in blood. While normal blood glucose levels range between 70 mg/dL (3.9 mM) and 140 mg/dL (7.8 mM) or higher, by contrast, tear glucose levels are on the order of 0.1–0.6 mM,[37−39] sweat glucose has been reported at 5 to 20 mg/dL (0.277−1.11 mM),[18] and saliva glucose concentrations are around 0.51−2.32 mg/dL (28.3 μM to 0.129 mM).[40−42] Figure 5a, b, and c show the representative current responses of the glucose in artificial human tears, artificial human sweat, and saliva, respectively. The details about the preparation of the body fluids are described in the Experimental Methods section. Initially, in Figure 5a, the devices were submerged in 0.1× PBS to obtain the baseline current. After changing the electrolyte from 0.1× PBS to artificial tears at 150 s, the sensing signal bumped up a little bit, which is due to the pH difference between artificial tears and 0.1× PBS. Noise levels of the glucose sensing in artificial tears were higher than the results in PBS when comparing the inset figures in Figure 4f and Figure 5a. This high noise level comes from the weaker buffer capability of the artificial tears and results in a lower signal-to-noise ratio, which consequently affects the detection limit. We extracted the relationship between the glucose concentration and the saturated current response from the real-time sensing data in PBS solution and plotted it in Figure 5d. For comparison, the sensing results in artificial tears, sweat, and saliva are also plotted. The high agreement between the data with PBS and the data with artificial tears is a good indicator that the signals from both media are attributed to mainly glucose instead of other nonspecific proteins. In the cases of artificial sweat and saliva, even though the sensing signals are slightly lower than
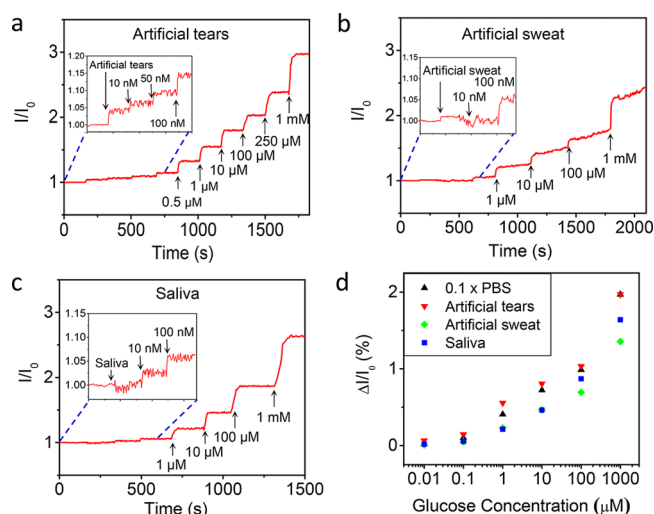

Figure 5. Glucose sensing in human body fluids. (a) Real-time glucose-sensing results in artificial tears. (b) Real-time glucose-sensing results in artificial sweat. (c) Real-time glucose sensing in human saliva. (d) Comparison of sensing responses *versus* different glucose concentrations in 0.1× PBS, artificial tears, artificial sweat, and saliva.

the responses from PBS, which may be due to their different ionic strengths and complex ingredients, our sensors can differentiate a glucose concentration as low as 0.1 μM. This sensitivity is sufficient to detect glucose in both sweat and saliva.

The In_2O_3 biosensors can be comfortably attached onto an artificial eyeball and an artificial arm (Figure 6a). To ensure the on-body sensing ability, we imitated the data collection on an artificial eyeball with the biosensor facing out. Figure 6b shows the *ex situ* glucose-sensing results using artificial tears. After using indium wires to connect the bonding pads to our measurement unit, we constantly flowed artificial tears through the sensing area, as shown in the inset of Figure 6b. After obtaining a stable baseline current, we sequentially flowed artificial tears spiked with 0.01, 0.1, 1, 10, 100, and 1000 μM glucose, respectively. Overall, it demonstrates that our wearable glucose-sensing platform has the potential to work as contact lenses with embedded sensors for monitoring the tear glucose level. Similarly, we performed glucose sensing on an artificial arm, but with the sensor facing down on the skin. As the sensing results shown in Figure 6c show, our In_2O_3 biosensor can work as a sweat patch for glucose monitoring. To further confirm that our sensing platform can be utilized as a wearable sweat analyzer, we collected sweat samples from a human subject's forehead during exercise. After we spiked the real sweat with different concentrations of glucose, glucose sensing was performed with the prepared samples. Figure 6d shows the sensing results with real sweat. After we added real sweat to replace the PBS solution, the sensing signal shows a large increase, which is because the original real sweat sample has a different pH and contains glucose before spiking. Good sensitivity was observed ranging from 0.1 μM to 1 mM, indicating that our sensing platform is a great candidate for wearable sweat analysis. We also measured sweat glucose levels before and after a meal for a healthy person. The before- and after-meal sweat sample were collected 30 min before and 30 min after a glucose beverage intake. The sensing results are shown in Figure 6e; the inset figure shows the device transfer
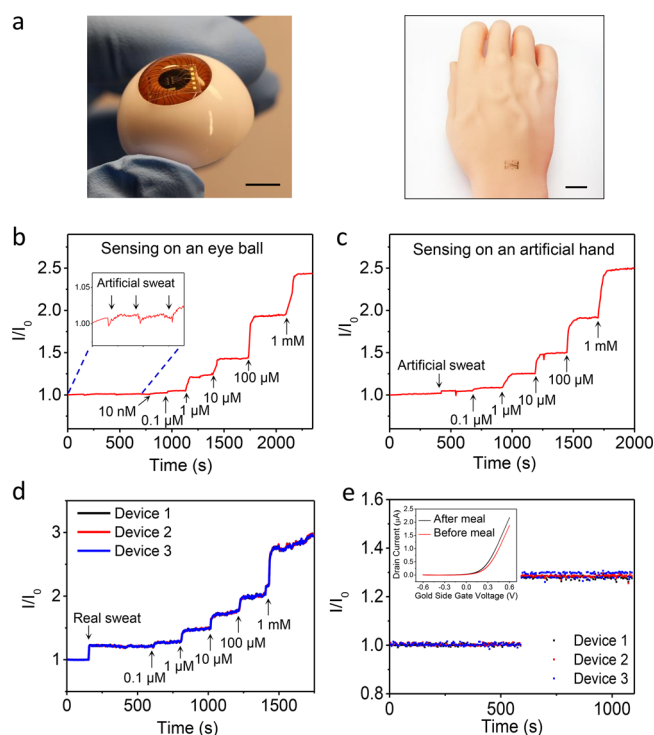
Figure 6. Off-body glucose sensing. (a) Photographs of the In_2O_3 biosensors attached onto an eyeball replica and an artificial arm. (b) Real-time glucose-sensing results on an artificial eyeball. (c) Real-time glucose-sensing results on an artificial arm. (d) Real-time glucose sensing with real sweat collected from human subjects. (e) Glucose-sensing results of real sweat collected before and after glucose beverage intake.

curve measured using before-meal and after-meal sweat samples as electrolyte. The subject's blood sugar level before and after a meal is also recorded using a commercial glucose meter, giving readings of 79 and 118 mg/dL, respectively.

We previously demonstrated that our In_2O_3 biosensors showed a very stable performance when they were kept in aqueous solutions.[27] However, the proteins such as glucose oxidase may not be as robust as the sensors after a long time.[43] We characterized an In_2O_3 biosensor with functionalization (chitosan/CNT/GOx) for 2 weeks. The device was measured every day and was stored at 4 °C after each measurement. The sensing signals showed only very small differences in the first 4 days, and the responses to 10 and 100 μM glucose in PBS decreased only about 25% and 30% after 2 weeks, respectively (Figure S8 in the Supporting Information). The decrease of the sensing responses can be attributed to the deactivation of the enzyme glucose oxidase and the loss of the enzymes during washing steps. The degradation of the devices would not be a problem in consideration of our low-cost disposable biosensors.

Wearable biosensors have great potential to be widely used in healthcare and fitness applications. Many groups have experimentally demonstrated functional prototypes. For example, Gao et al. made great progress and developed a wearable sensor platform for multiplexed in situ perspiration analysis.[2] The reported potentiometric biosensor arrays can detect a wide variety of sweat metabolites and electrolytes, including glucose. Lee et al. have introduced a "patch-like" electrochemical device for diabetes monitoring and therapy.[44] In this work, we demonstrated a FET-based prototype glucose biosensor using In_2O_3 nanoribbons, which can be comple-

mentary to electrochemical sensors. The facile and low-temperature shadow-mask fabrication process can produce wearable biosensors with high sensitivity (~10 nM detection limit) and a wide detection range (~5 orders of magnitude). Moreover, our biosensor platform can be easily integrated with digital wristbands, smart watches, and implantable electronics.

Recently, great progress has been made using liquid metal-based reaction to produce 2D semiconductors.[45−47] Because of their good charge-carrier mobility and outstanding mechanical properties, 2D materials are very promising for next-generation wearable electronics. Wearable biosensors using single-crystalline, sub-nanometer layers of 2D materials, such as In_2O_3, Ga_2O_3, SnO_2, ZnO, and InGaZnO, can be explored in the future.

CONCLUSIONS

In summary, the In_2O_3 FET-based wearable biosensors with on-chip gold side gate electrodes can be used for highly sensitive detection of glucose with a detection limit down to 10 nM. The all-on-a-chip device structure can be incorporated into a straightforward two-step shadow-mask fabrication. The gold side gate electrodes show a stable and efficient gating effect on In_2O_3 FETs on flexible substrates. Mobilities in 0.1× PBS of ~22 cm^2 V^{-1} s^{-1} and on−off ratios of more than 10^5 were achieved. The noninvasive glucose detection in human body fluids, such as tears and sweat, was also demonstrated. We further investigated glucose sensing on an eyeball replica and on an artificial hand. Lastly, we demonstrated that our glucose sensor can work in real human sweat and can distinguish glucose levels before and after a meal. Given the facile and highly scalable fabrication process, low driving voltage, and reliable sensing behavior even when deformed, this sensing platform is promising for continuous personalized health monitoring, for the food industry, and for environmental monitoring.

EXPERIMENTAL METHODS

Fabrication Process. A PET substrate was first cleaned with acetone and isopropyl alcohol and then went through ultraviolet treatment before the fabrication process. After the cleaning process, the first shadow mask was attached to the PET substrate to define the channel area. Then In_2O_3 nanoribbons were deposited by RF sputtering (Denton Discovery 550 sputtering system). By simply detaching the shadow mask, we got well-patterned nanoribbons. The source, drain, and gold side electrodes were then defined by the second shadow mask, followed by electron beam evaporation of 1 nm Ti and 50 nm Au. After deposition, the shadow mask was removed.

Characterization. Optical microscopy images were taken with an Olympus microscope. The SEM images were taken with a Hitachi S-4800 field emission scanning electron microscope. Electrical characteristics and sensing results were measured with an Agilent 1500B semiconductor analyzer.

Device Functionalization. Chitosan powder (1 wt %) was first dissolved in a 2 wt % acetic acid aqueous solution. Next, the chitosan solution was mixed with single-walled carbon nanotubes (2 mg mL^{-1} in 1× PBS) using ultrasonication for over 30 min. The chitosan/SWCNT solution was mixed with a glucose oxidase solution (10 mg mL^{-1} in 1× PBS) in the volume ratio of 2:1. The mixed solution was then inkjet printed onto the source and drain electrodes and dried under ambient conditions.

Human Body Fluid Samples. Artificial human tear solution was bought from Walgreens. Artificial human sweat was prepared by mixing 22 mM urea, 5.5 mM lactic acid, 3 mM NH_4^+, 100 mM Na^+, 10 mM K^+, 0.4 mM Ca^{2+}, 50 μM Mg^{2+}, and 25 μM uric acid with varying

glucose concentrations.[2] Real sweat samples were collected from humans by scratching their foreheads with microtubes.

ASSOCIATED CONTENT

Ⓢ Supporting Information

The Supporting Information is available free of charge on the ACS Publications website at DOI: 10.1021/acsnano.7b06823.

> AFM and XRD characterization; mobility calculation; statistical study; bending test; tensile strain calculation; pH sensing; glucose-sensing control experiment; stability tests (PDF)

AUTHOR INFORMATION

Corresponding Authors
*E-mail: chongwuz@usc.edu.
*E-mail: mamer@seas.ucla.edu.

ORCID 🟢
Yihang Liu: 0000-0002-2491-9439
Moh R. Amer: 0000-0003-3318-2667
Chongwu Zhou: 0000-0001-8448-8450

Notes
The authors declare no competing financial interest.

REFERENCES

(1) Takei, K.; Takahashi, T.; Ho, J. C.; Ko, H.; Gillies, A. G.; Leu, P. W.; Fearing, R. S.; Javey, A. Nanowire Active-Matrix Circuitry for Low-Voltage Macroscale Artificial Skin. *Nat. Mater.* **2010**, *9*, 821−826.

(2) Gao, W.; Emaminejad, S.; Nyein, H. Y. Y.; Challa, S.; Chen, K.; Peck, A.; Fahad, H. M.; Ota, H.; Shiraki, H.; Kiriya, D.; Lien, D.; Brooks, G. A.; Davis, R. W.; Javey, A. Fully Integrated Wearable Sensor Arrays for Multiplexed *in Situ* Perspiration Analysis. *Nature* **2016**, *529*, 509−514.

(3) Kaltenbrunner, M.; Sekitani, T.; Reeder, J.; Yokota, T.; Kuribara, K.; Tokuhara, T.; Drack, M.; Schwödiauer, R.; Graz, I.; Bauer-Gogonea, S.; Bauer, S.; Someya, T. An Ultra-Lightweight Design for Imperceptible Plastic Electronics. *Nature* **2013**, *499*, 458−463.

(4) Xu, S.; Zhang, Y.; Jia, L.; Mathewson, K. E.; Jang, K.-I.; Kim, J.; Fu, H.; Huang, X.; Chava, P.; Wang, R.; Bhole, S.; Wang, L.; Na, Y. J.; Guan, Y.; Flavin, M.; Han, Z.; Huang, Y.; Rogers, J. A.,Soft Microfluidic Assemblies of Sensors, Circuits, and Radios for the Skin. *Science* **2014**, *344*, 70−74.

(5) McAlpine, M. C.; Ahmad, H.; Wang, D.; Heath, J. R. Highly Ordered Nanowire Arrays on Plastic Substrates for Ultrasensitive Flexible Chemical Sensors. *Nat. Mater.* **2007**, *6*, 379−384.

(6) Kim, D. H.; Lu, N.; Ma, R.; Kim, Y. S.; Kim, R. H.; Wang, S.; Wu, J.; Won, S. M.; Tao, H.; Islam, A.; Yu, K. J.; Kim, T. I.; Chowdhury, R.; Ying, M.; Xu, L.; Li, M.; Chung, H. J.; Keum, H.; McCormick, M.; Liu, P.; et al. Epidermal Electronics. *Science* **2011**, *333*, 838−843.

(7) Lipomi, D. J.; Vosgueritchian, M.; Tee, B. C.; Hellstrom, S. L.; Lee, J. A.; Fox, C. H.; Bao, Z. Skin-Like Pressure and Strain Sensors Based on Transparent Elastic Films of Carbon Nanotubes. *Nat. Nanotechnol.* **2011**, *6*, 788−792.

(8) Lee, H.; Song, C.; Hong, Y. S.; Kim, M. S.; Cho, H. R.; Kang, T.; Shin, K.; Choi, S. H.; Hyeon, T.; Kim, D. H. Wearable/Disposable Sweat-Based Glucose Monitoring Device with Multistage Transdermal Drug Delivery Module. *Sci. Adv.* **2017**, *3*, 3.

(9) Bandodkar, A. J.; Wang, J. Non-Invasive Wearable Electrochemical Sensors: A Review. *Trends Biotechnol.* **2014**, *32*, 363−371.

(10) Makaram, P.; Owens, D.; Aceros, J. Trends in Nanomaterial-Based Non-Invasive Diabetes Sensing Technologies. *Diagnostics* **2014**, *4*, 27−46.

(11) Mannoor, M. S.; Tao, H.; Clayton, J. D.; Sengupta, A.; Kaplan, D. L.; Naik, R. R.; Verma, N.; Omenetto, F. G.; McAlpine, M. C. Graphene-Based Wireless Bacteria Detection on Tooth Enamel. *Nat. Commun.* **2012**, *3*, 763.

(12) Liao, C.; Mak, C.; Zhang, M.; Chan, H. L.; Yan, F. Flexible Organic Electrochemical Transistors for Highly Selective Enzyme Biosensors and Used for Saliva Testing. *Adv. Mater.* **2015**, *27*, 676−681.

(13) Veiseh, O.; Tang, B. C.; Whitehead, K. A.; Anderson, D. G.; Langer, R. Managing Diabetes with Nanomedicine: Challenges and Opportunities. *Nat. Rev. Drug Discovery* **2015**, *14*, 45−57.

(14) Olarte, O.; Chilo, J.; Pelegri-Sebastia, J.; Barbe, K.; Van Moer, W. Glucose Detection in Human Sweat Using An Electronic Nose. *Conf. Proc. IEEE Eng. Med. Biol. Soc.* **2013**, 1462−1465.

(15) Yan, Q.; Peng, B.; Su, G.; Cohan, B. E.; Major, T. C.; Meyerhoff, M. E. Measurement of Tear Glucose Levels with Amperometric Glucose Biosensor/Capillary Tube Configuration. *Anal. Chem.* **2011**, *83*, 8341−8346.

(16) Vashist, S. K. Non-Invasive Glucose Monitoring Technology in Diabetes Management: A Review. *Anal. Chim. Acta* **2012**, *750*, 16−27.

(17) Tierney, M.; Kim, H.; Burns, M.; Tamada, J.; Potts, R. Electroanalysis of Glucose in Transcutaneously Extracted Samples. *Electroanalysis* **2000**, *12*, 666−671.

(18) Moyer, J.; Wilson, D.; Finkelshtein, I.; Wong, B.; Potts, R. Correlation between Sweat Glucose and Blood Glucose in Subjects with Diabetes. *Diabetes Technol. Ther.* **2012**, *14*, 398−402.

(19) Ronkainen, N. J.; Halsall, H. B.; Heineman, W. R. Electro-chemical Biosensors. *Chem. Soc. Rev.* **2010**, *39*, 1747−1763.

(20) Zhang, M.; Liao, C.; Mak, C. H.; You, P.; Mak, C. L.; Yan, F. Highly Sensitive Glucose Sensors Based on Enzyme-Modified Whole-Graphene Solution-Gated Transistors. *Sci. Rep.* **2015**, *5*, 8311.

(21) Zhai, D.; Liu, B.; Shi, Y.; Pan, L.; Wang, Y.; Li, W.; Zhang, R.; Yu, G. Highly Sensitive Glucose Sensor Based on Pt Nanoparticle/Polyaniline Hydrogel Heterostructures. *ACS Nano* **2013**, *7*, 3540−3546.

(22) Lin, P.; Yan, F.; Chan, H. L. Ion-Sensitive Properties of Organic Electrochemical Transistors. *ACS Appl. Mater. Interfaces* **2010**, *2*, 1637−1641.

(23) Claussen, J. C.; Kumar, A.; Jaroch, D. B.; Khawaja, M. H.; Hibbard, A. B.; Porterfield, D. M.; Fisher, T. S. Nanostructuring Platinum Nanoparticles on Multilayered Graphene Petal Nanosheets for Electrochemical Biosensing. *Adv. Funct. Mater.* **2012**, *22*, 3399−3405.

(24) Tang, H.; Yan, F.; Lin, P.; Xu, J.; Chan, H. L. Highly Sensitive Glucose Biosensors Based on Organic Electrochemical Transistors Using Platinum Gate Electrodes Modified with Enzyme and Nanomaterials. *Adv. Funct. Mater.* **2011**, *21*, 2264−2272.

(25) Heller, A. Implanted Electrochemical Glucose Sensors for the Management of Diabetes. *Annu. Rev. Biomed. Eng.* **1999**, *1*, 153−175.

(26) Liu, Q.; Aroonyadet, N.; Song, Y.; Wang, X.; Cao, X.; Liu, Y.; Cong, S.; Wu, F.; Thompson, M. E.; Zhou, C. Highly Sensitive and Quick Detection of Acute Myocardial Infarction Biomarkers Using In$_2$O$_3$ Nanoribbon Biosensors Fabricated Using Shadow Masks. *ACS Nano* **2016**, *10*, 10117−10125.

(27) Aroonyadet, N.; Wang, X.; Song, Y.; Chen, H.; Cote, R. J.; Thompson, M. E.; Datar, R. H.; Zhou, C. Highly Scalable, Uniform, and Sensitive Biosensors Based on Top-Down Indium Oxide Nanoribbons and Electronic Enzyme-Linked Immunosorbent Assay. *Nano Lett.* **2015**, *15*, 1943−1951.

(28) Rim, Y. S.; Bae, S. H.; Chen, H.; Yang, J. L.; Kim, J.; Andrews, A. M.; Weiss, P. S.; Yang, Y.; Tseng, H.-R. Printable Ultrathin Metal Oxide Semiconductor-Based Conformal Biosensors. *ACS Nano* **2015**, *9*, 12174−12181.

(29) Kim, J.; Rim, Y. S.; Chen, H.; Cao, H. H.; Nakatsuka, N.; Hinton, H. L.; Zhao, C.; Andrews, A. M.; Yang, Y.; Weiss, P. S. Fabrication of High-Performance Ultrathin In$_2$O$_3$ Film Field-Effect

Transistors and Biosensors Using Chemical Lift-Off Lithography. *ACS Nano* **2015**, *9*, 4572−4582.

(30) Tang, T.; Han, S.; Jin, W.; Liu, X.; Li, C.; Zhang, D.; Zhou, C.; Chen, B.; Han, J.; Meyyapan, M. Synthesis and Characterization of Single-Crystal Indium Nitride Nanowires. *J. Mater. Res.* **2004**, *19*, 423−426.

(31) Cao, X.; Cao, Y.; Zhou, C. Imperceptible and Ultraflexible p-Type Transistors and Macroelectronics Based on Carbon Nanotubes. *ACS Nano* **2016**, *10*, 199−206.

(32) Someya, T.; Kato, Y.; Sekitani, T.; Iba, S.; Noguchi, Y.; Murase, Y.; Kawaguchi, H.; Sakurai, T. Conformable, Flexible, Large-Area Networks of Pressure and Thermal Sensors with Organic Transistor Active Matrixes. *Proc. Natl. Acad. Sci. U. S. A.* **2005**, *102*, 12321−12325.

(33) Abbas, A. N.; Liu, G.; Liu, B.; Zhang, L.; Liu, H.; Ohlberg, D.; Wu, W.; Zhou, C. Patterning, Characterization, and Chemical Sensing Applications of Graphene Nanoribbon Arrays Down to 5 nm Using Helium Ion Beam Lithography. *ACS Nano* **2014**, *8*, 1538−1546.

(34) Park, S.; Lee, S.; Kim, C.-H.; Lee, I.; Lee, W.-J.; Kim, S.; Lee, B.-G.; Jang, J.-H.; Yoon, M.-H. Sub-0.5 V Highly Stable Aqueous Salt Gated Metal Oxide Electronics. *Sci. Rep.* **2015**, *5*, 13088.

(35) Hrapovic, S.; Liu, Y.; Male, K. B.; Luong, J. H. Electrochemical Biosensing Platforms Using Platinum Nanoparticles and Carbon Nanotubes. *Anal. Chem.* **2004**, *76*, 1083−1088.

(36) Wang, J.; Musameh, M.; Lin, Y. Solubilization of Carbon Nanotubes by Nafion toward the Preparation of Amperometric Biosensors. *J. Am. Chem. Soc.* **2003**, *125*, 2408−2409.

(37) Berman, E. R. *Biochemistry of the Eye*; Plenum Press: New York, 1991

(38) Yao, H.; Shum, A. J.; Cowan, M.; Lähdesmäki, I.; Parviz, B. A. A Contact Lens with Embedded Sensor for Monitoring Tear Glucose Level. *Biosens. Bioelectron.* **2011**, *26*, 3290−3296.

(39) Yao, H.; Liao, Y.; Lingley, A.; Afanasiev, A.; Lähdesmäki, I.; Otis, B.; Parviz, B. A Contact Lens with Integrated Telecommunication Circuit and Sensors for Wireless and Continuous Tear Glucose Monitoring. *J. Micromech. Microeng.* **2012**, *22*, 075007.

(40) Abikshyeet, P.; Ramesh, V.; Oza, N. Glucose Estimation in the Salivary Secretion of Diabetes Mellitus Patients. *Diabetes, Metab. Syndr. Obes.: Targets Ther.* **2012**, *5*, 149.

(41) Zhang, W.; Du, Y.; Wang, M. L. Noninvasive Glucose Monitoring Using Saliva Nano-Biosensor. *Sens. Bio-Sensing Res.* **2015**, *4*, 23−29.

(42) Zhang, W.; Du, Y.; Wang, M. L. On-Chip Highly Sensitive Saliva Glucose Sensing Using Multilayer Films Composed of Single-Walled Carbon Nanotubes, Gold Nanoparticles, and Glucose Oxidase. *Sens. Bio-Sensing Res.* **2015**, *4*, 96−102.

(43) Valdes, T. I.; Moussy, F. *In Vitro* and *in Vivo* Degradation of Glucose Oxidase Enzyme Used for an Implantable Glucose Biosensor. *Diabetes Technol. Ther.* **2000**, *2*, 367−376.

(44) Lee, H.; Choi, T. K.; Lee, Y. B.; Cho, H. R.; Ghaffari, R.; Wang, L.; Choi, H. J.; Chung, T. D.; Lu, N.; Hyeon, T. A Graphene-Based Electrochemical Device with Thermoresponsive Microneedles for Diabetes Monitoring and Therapy. *Nat. Nanotechnol.* **2016**, *11*, 566−572.

(45) Zavabeti, A.; Ou, J. Z.; Carey, B. J.; Syed, N.; Orrell-Trigg, R.; Mayes, E. L.; Xu, C.; Kavehei, O.; O'mullane, A. P.; Kaner, R. B. A Liquid Metal Reaction Environment for the Room-Temperature Synthesis of Atomically Thin Metal Oxides. *Science* **2017**, *358*, 332−335.

(46) Kim, Y. D.; Hone, J. Materials Science: Screen Printing of 2D Semiconductors. *Nature* **2017**, *544*, 167−168.

(47) Carey, B. J.; Ou, J. Z.; Clark, R. M.; Berean, K. J.; Zavabeti, A.; Chesman, A. S.; Russo, S. P.; Lau, D. W.; Xu, Z.-Q.; Bao, Q. Wafer-scale two-dimensional semiconductors from printed oxide skin of liquid metals. *Nat. Commun.* **2017**, *8*, 14482.